

Variability of the Human Cardiac Laminar Structure

Herve Lombaert^{1,2}, Jean-Marc Peyrat⁴, Laurent Fanton³, Farida Cheriet²,
Hervé Delingette¹, Nicholas Ayache¹, Patrick Clarysse³, Isabelle Magnin³,
Pierre Croisille³

¹ INRIA, Asclepios Team, Sophia-Antipolis, France

² École Polytechnique de Montréal, Canada

³ CREATIS, Université de Lyon, France

⁴ Siemens Molecular, Oxford, UK

Abstract. The cardiac fiber architecture has an important role in electrophysiology, in mechanical functions of the heart, and in remodeling processes. The variability of the fibers is the focus of various studies in different species. However, the variability of the laminar sheets is still not well known especially in humans. In this paper, we present preliminary results on a quantitative study on the variability of the human cardiac laminar structure. We show that the laminar structure has a complex variability and we show the possible presence of two populations of laminar sheets. Bimodal distributions of the intersection angle of the third eigenvector of the diffusion tensor have been observed in 10 *ex vivo* healthy human hearts. Additional hearts will complete the study and further characterize the different populations of cardiac laminar sheets.

1 Introduction

The heart is a complex muscle that is composed with myocardial fibers organized as laminar sheets [25,16]. The cardiac fiber structures have an important role in electrophysiology [14] and in mechanical functions [6] of the heart. The understanding of the cardiac fiber architecture is essential for better diagnosis and treatment of many cardiac pathologies. The fibrous nature of the heart has been known for centuries, tracing back to as early as 1694 [28], but has been limited to tedious histological studies [20]. The cardiac fiber structure can now be imaged with diffusion tensor magnetic resonance imaging (DT-MRI) [2,15], however the variability of the fiber structure in humans is still not well known (due to the very limited number and the value of post-mortem healthy human hearts) and is largely speculated from studies on other species (dogs [12,13,11,26,22,21,9], goats [8], and rats [3]). Recently, Lombaert *et al.* [17,18] constructed a statistical atlas of the human cardiac fiber architecture and assessed its variability. The fiber structure is shown to be more stable than the laminar sheet structure. They hypothesized that the higher variability of the laminar sheet could be due to the presence of two or more populations of laminar sheets [11]. Helm *et al.*

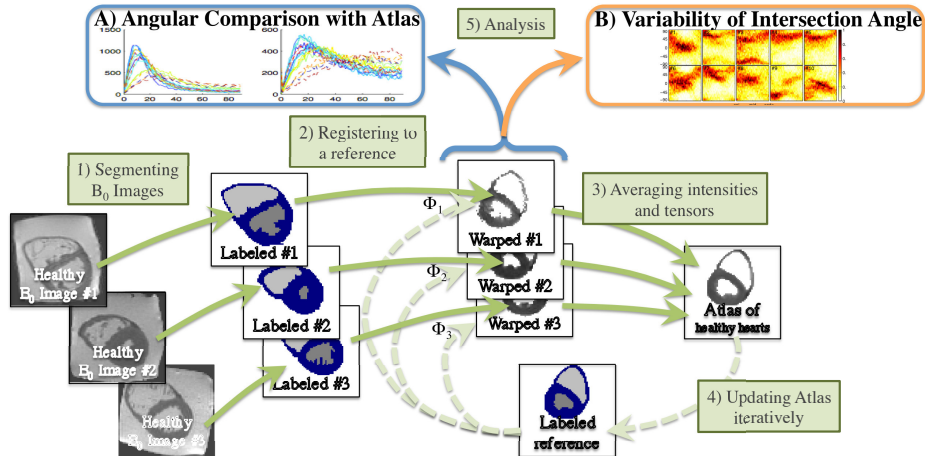


Fig. 1: *Atlas Construction*: (1) From the acquired images, the myocardia are segmented. (2) Images are then aligned and registered non-rigidly toward a reference image. (3,4) The atlas is constructed iteratively by averaging acquired images in the average heart shape. *Variability of the laminar sheets*: (A) The directions of the laminar sheet normals are compared with the atlas for each heart, and (B) the probability distribution of the intersection angle is analyzed.

studied the variability of the cardiac laminar sheet in [13]. Using 7 canine hearts, they observed a bimodal distribution of intersection angles (i.e., two populations of laminar sheet structure) in most myocardial segments of the left ventricle.

We present here the preliminary results of a study on the variability of the cardiac laminar sheet structure in humans. The methods used to construct and analyze the statistical atlas are briefly described. Next, the results show the angular variability, from the average healthy heart, of the the laminar sheet normal. The complexity of the laminar sheet structure is revealed thereafter by analyzing the distribution of the intersection angle of the laminar sheet normal. The distributions suggest the possible presence of two populations of laminar sheets in several myocardial segments of the left ventricle.

2 Material and Method

2.1 Dataset

The human dataset [7,23] consists of 10 healthy *ex vivo* human hearts acquired during forensic autopsies. The excised hearts were placed in a plastic container and filled with non destructive hydrophilic gel to maintain a diastolic shape. The images have been acquired on a 1.5T MR scanner (Avanto Siemens), all within 24 hours after death and prior to the examination by the pathologist, with a bipolar echo planar imaging using 4 repetitions of 12 gradient images. The

diffusion-weighted images, from which are estimated the diffusion tensors, are of size 128x128x52 with an isotropic resolution of 2 mm. All cases are from extra cardiac sudden deaths, and the hearts are classified as healthy after controlling their weight, wall thickness, and subsequent pathology examination [24].

2.2 Atlas Construction

The statistical atlas is constructed using four steps, all fully described in [17] and summarized here in Fig. 1. Information on the fiber architecture (i.e., any directional data from DT-MRI) is purposely omitted from the registration process in order to avoid introducing any bias in the study of the fiber variability.

Myocardium Segmentation — *Firstly*, the myocardium of each heart is segmented out on the B_0 image of the DT-MRI acquisition. The segmentation method is based on Graph Cuts [4].

Heart Registration — *Secondly*, each myocardium is registered to a reference image using solely the B_0 images and the myocardial masks. The pairwise registrations are performed with the symmetric Log-domain diffeomorphic demons [29,19].

Construction of Healthy Atlas — *Thirdly*, the reference image is deformed toward the morphological average of all hearts by iterating until convergence the pairwise registrations and the heart averaging steps. This atlas construction follows Guimond’s *et al.* method [10].

Warping of Diffusion Tensors — *Fourthly*, and last, the resulting deformation fields computed from the registration process are used to warp all tensor fields to the morphological atlas. The diffusion tensors are reoriented using the Finite Strain strategy since it preserves the geometric features [22].

2.3 Statistical Analysis

The diffusion tensor space of symmetric positive definite matrices does not have a vector space structure with the standard Euclidean metric. The Log-Euclidean metric [1] provides a simple and fast framework where first order arithmetic on diffusion tensors has a closed form solution. The average diffusion tensor field, $\bar{\mathbf{D}}$, is computed from the N warped tensor fields $\{\mathbf{D}^{(i)}\}_{i=1\dots N}$ (with $N = 10$ healthy hearts) using the Fréchet mean:

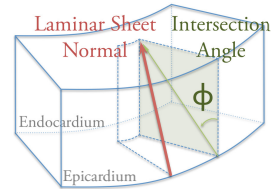
$$\bar{\mathbf{D}} = \exp \left(\frac{1}{N} \sum_{i=1}^N \log(\mathbf{D}^{(i)}) \right) \quad (1)$$

The eigendecomposition of the average diffusion tensor $\bar{\mathbf{D}}$ gives the three average eigenvectors $\bar{\mathbf{v}}_{1,2,3}$. The maximal local diffusion, revealed by the primary eigenvector \mathbf{v}_1 occurs along the fiber while most of the remaining diffusion occurs within the laminar sheet, where the secondary eigenvector \mathbf{v}_2 is thought to lay [12,13,27]. The tertiary eigenvector, \mathbf{v}_3 , corresponds to the normal of the laminar sheet.

The deviation of the cardiac laminar sheet of each heart is given with the angular difference θ from the direction of laminar sheet normal, \mathbf{v}_3 , to the direction of the average laminar sheet normal, $\bar{\mathbf{v}}_3$. For instance, for the i^{th} heart, the angular deviation from the average heart is:

$$\theta_3^{(i)} = \arccos \left(\frac{|\mathbf{v}_3^{(i)} \cdot \bar{\mathbf{v}}_3|}{\|\mathbf{v}_3^{(i)}\| \|\bar{\mathbf{v}}_3\|} \right) \quad (2)$$

The angles are defined between 0° and 90° . The absolute value of the dot product removes the inherent ambiguity in the orientation of the eigenvectors (i.e., $|a \cdot b| = |a \cdot (-b)|$). The variability of the laminar sheet can be measured with the probability distribution of the intersection angle of the third eigenvector (i.e., of the laminar sheet normal). The intersection angle [16] is defined as the projected angle of the laminar sheet normal (in red in the right figure) onto a transverse plane (the vertical transmural plane in green in the right figure). A prolate ellipsoidal model of the heart [20] is fitted to the morphology of the statistical atlas to ease measurements in the prolate ellipsoidal coordinates.



Intersection angle of the 3rd eigenvector in a myocardial section.

3 Results

The cardiac laminar sheet was shown [17] to vary more than the fiber direction. In order to understand the higher variability, the distribution of the intersection angle of the laminar sheet normal is estimated in all hearts and in several myocardial segments. The distributions show the presence of possibly two populations of laminar sheets.

3.1 Variability of the Laminar Sheet Normal

The direction of the laminar sheet normal in each heart is compared with the ones of the average healthy heart (i.e., the atlas). The angular differences of the laminar sheet normals, given by Eq. 2 and shown in Fig. 3, present deviations to the average heart in several areas for each heart. The histogram of the angular differences, in Fig. 2, shows an angular peak at $\bar{\theta}_3 = 15.77^\circ$ (the average of the histogram modes in Fig. 2).

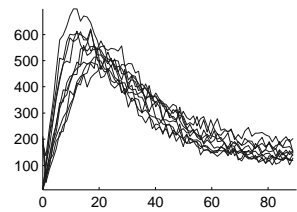


Fig. 2: Histograms of the angular deviation θ_3 (in degrees) for 10 hearts.

3.2 Variability of the Intersection Angle

We now study the probability distribution of the intersection angle of the third eigenvector (i.e., the laminar sheet normal). The probability distributions are

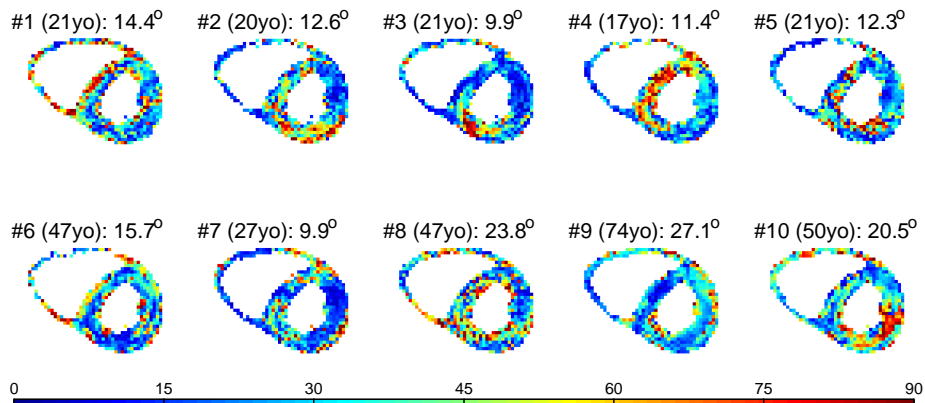


Fig. 3: Deviation, θ_3 , of the laminar sheet normal of each heart to the atlas. The coloring is the angular difference in degree.

presented in a joint histograms (Fig. 4) where the angle distribution, on the vertical axis, is plotted against all transmural distances, on the horizontal axis. Each heart appears to have a consistent distribution of laminar sheet normal directions with angles concentrated around a specific mean. Subject #3, #6, #9, and #10 appear to show two populations of laminar sheet normals (i.e., the angles are concentrated along two horizontal curves). The global joint histogram in Fig. 4(b) shows the probability distribution of the intersection angle (i.e., the variability of the laminar sheet normal) among all 10 hearts. Furthermore, the probability distributions in the 17 AHA segments (American Heart Association [5]) provide local statistics across the myocardium. More distinct clusters of laminar sheet structures are visible in Fig. 5, in particular AHA zones 2, 3, 4, 7, 8, 9, 12, 13, and 14 show angular distributions concentrated along two horizontal curves. These curves of average angles can be estimated using Gaussian Mixture Models (i.e., for each transmural distance, the intersection angle values are clustered into two Gaussian models). This is illustrated with two blue curves in each joint histogram. Each curves indicates the estimated mean angle of one of the two Gaussian models.

4 Conclusion

In this paper, preliminary results of a study on variability of the human cardiac laminar structure have been presented. The cardiac fiber architecture has an important role in electrophysiology and in mechanical functions of the heart. The variability of the laminar sheets in humans is still not well known. It is thought that there are two populations of laminar sheets. Helm *et al.* [13] observed in 7 canine hearts a bimodal distribution of intersection angles of the third eigenvector (i.e., the laminar sheet normal). We similarly observed a bimodal distribution of intersection angles in human hearts. Our preliminary results within the dataset

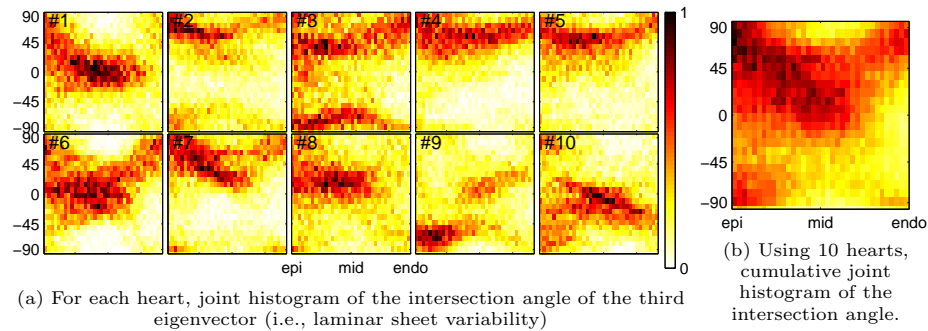


Fig. 4: Joint histograms showing the distribution of the intersection angle from epicardium (*left side of each histogram*) to endocardium (*right side of each histogram*) for (a) each heart, and (b) all hearts combined. The x -axis is the transmural distance from epicardium. The y -axis is the distribution of the intersection angles observed at one specific transmural distance (i.e., each column is the histogram of angles for one given distance). Color is the normalized probability distribution.

of 10 hearts suggest the possible presence of two populations of laminar sheets. We will include additional hearts to the study and try to further characterize the different populations of cardiac laminar sheets.

Acknowledgment

The authors wish to acknowledge helpful comments from Leon Axel and the members of the Asclepios Team. The project was supported financially by the National Science and Engineering Research Council of Canada (NSERC), the Michael Smith Scholarship (CGS-MSFSS), and the EGIDE/INRIA Scholarship.

References

1. V. Arsigny, P. Fillard, X. Pennec, and N. Ayache. Log-Euclidean metrics for fast and simple calculus on diffusion tensors. *MRM*, 56(2):411–421, 2006.³
2. P. J. Basser, J. Mattiello, and D. LeBihan. MR diffusion tensor spectroscopy and imaging. *Biophysical Journal*, 66(1):259–267, 1994.¹
3. M. Bishop, P. Hales, G. Plank, D. Gavaghan, J. Scheider, and V. Grau. Comparison of Rule-Based and DTMRI-Derived Fibre Architecture in a Whole Rat Ventricular Computational Model. In *FIMH*, pages 87–96, 2009.¹
4. Y. Boykov and M.-P. Jolly. Interactive Organ Segmentation Using Graph Cuts. In *MICCAI*, pages 276–286, 2000.³
5. M. D. Cerqueira, N. J. Weissman, V. Dilsizian, A. K. Jacobs, S. Kaul, W. K. Laskey, D. J. Pennell, J. A. Rumberger, T. Ryan, and M. S. Verani. Standardized Myocardial Segmentation and Nomenclature for Tomographic Imaging of the

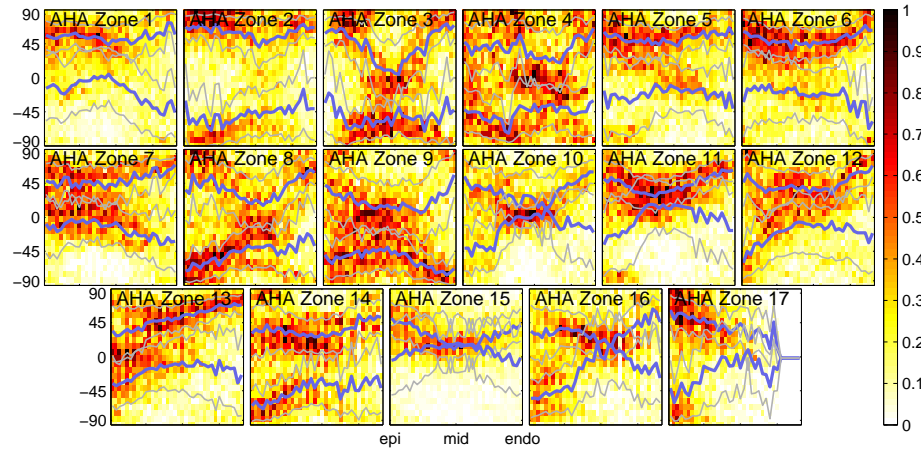


Fig. 5: Joint histograms showing of the distribution of the intersection angle in 17 AHA LV segments. Blue curves (mean angles) are found using GMM (gray lines are the one-standard-deviation envelopes). Two populations of intersection angles are visible in most segments.

- Heart: A Statement for Healthcare Professionals From the Cardiac Imaging Committee of the Council on Clinical Cardiology of the American Heart Association. *Circulation*, 105(4):539–542, 2002.⁵
6. K. D. Costa, J. W. Holmes, and A. D. McCulloch. Modelling cardiac mechanical properties in three dimensions. *Mathematical, Physical and Engineering Sciences*, 359(1783):1233–1250, 2001.¹
 7. C. Frindel, M. Robini, P. Croisille, and Y.-M. M. Zhu. Comparison of regularization methods for human cardiac diffusion tensor MRI. *Med. Im. An.*, 13(3), 2009.²
 8. L. Geerts, P. Bovendeerd, K. Nicolay, and T. Arts. Characterization of the normal cardiac myofiber field in goat measured with MR-diffusion tensor imaging. *Am. J. of Physiology - Heart and Circulatory Physiology*, 283(1):H139–H145, 2002.¹
 9. S. Gilbert, A. Benson, P. Li, and A. Holden. Visualisation of Dog Myocardial Structure from Diffusion Tensor Magnetic Resonance Imaging: The Paradox of Uniformity and Variability. In *FIMH*, pages 403–412, 2007.¹
 10. A. Guimond, J. Meunier, and J. P. Thirion. Average Brain Models: A Convergence Study. *CVIU*, pages 192–210, 2000.³
 11. P. A. Helm. *A novel technique for quantifying variability of cardiac anatomy: Application to the dyssynchronous failing heart*. PhD thesis, Johns Hopkins University, 2005.¹
 12. P. A. Helm, M. F. Beg, M. I. Miller, and R. L. Winslow. Measuring and mapping cardiac fiber and laminar architecture using diffusion tensor MR imaging. *Annals of the New York Academy of Sciences*, 1047:296–307, 2005.^{1, 3}
 13. P. A. Helm, H.-J. J. Tseng, L. Younes, E. R. McVeigh, and R. L. Winslow. Ex vivo 3D diffusion tensor imaging and quantification of cardiac laminar structure. *MRM*, 54(4):850–859, 2005.^{1, 2, 3, 5}

14. D. A. Hooks, K. A. Tomlinson, S. G. Marsden, I. J. LeGrice, B. H. Smaill, A. J. Pullan, and P. J. Hunter. Cardiac Microstructure: Implications for Electrical Propagation and Defibrillation in the Heart. *Circ. Res.*, 91(4):331–338, 2002.¹
15. E. W. Hsu and C. S. Henriquez. Myocardial fiber orientation mapping using reduced encoding diffusion tensor imaging. *Journal of Cardiovascular Magnetic Resonance*, 3(4):339–347, 2001.¹
16. I. J. LeGrice, B. H. Smaill, L. Z. Chai, S. G. Edgar, J. B. Gavin, and P. J. Hunter. Laminar structure of the heart: ventricular myocyte arrangement and connective tissue architecture in the dog. *Am. J. of physiology*, 269(2), 1995.^{1, 4}
17. H. Lombaert, J.-M. Peyrat, P. Croisille, S. Rapacchi, L. Fanton, P. Clarysse, H. Delingette, and N. Ayache. In *FIMH*, volume 6666, pages 171–179, 2011.^{1, 3, 4}
18. H. Lombaert, J.-M. Peyrat, S. Rapacchi, L. Fanton, H. Delingette, P. Croisille, P. Clarysse, and N. Ayache. In *ISMRM*, 2011.¹
19. T. Mansi, X. Pennec, M. Sermesant, H. Delingette, and N. Ayache. iLogDemons: A Demons-Based registration algorithm for tracking incompressible elastic biological tissues. *IJCV*, pages 1–20, 2010.³
20. P. M. Nielsen, I. J. Le Grice, B. H. Smaill, and P. J. Hunter. Mathematical model of geometry and fibrous structure of the heart. *Am. J. of Physiology, Heart Circulatory Physiology*, 260(4):H1365–1378, 1991.^{1, 4}
21. J. M. Peyrat. *Comparison of Cardiac Anatomy and Function: Statistics on Fibre Architecture from DT-MRI and Registration of 4D CT Images*. PhD thesis, Nice Sophia Antipolis University, 2009.¹
22. J.-M. Peyrat, M. Sermesant, X. Pennec, H. Delingette, C. Xu, E. R. McVeigh, and N. Ayache. A Computational Framework for the Statistical Analysis of Cardiac Diffusion Tensors: Application to a Small Database of Canine Hearts. *IEEE TMI*, 26(11):1500–1514, 2007.^{1, 3}
23. S. Rapacchi, P. Croisille, V. Pai, D. Grenier, M. Viallon, P. Kellman, N. Mewton, and H. Wen. Reducing motion sensitivity in free breathing DWI of the heart with localized Principal Component Analysis. In *ISMRM*, 2010.²
24. M. Silver, A. I. Gotlieb, and F. R. Schoen. *Cardiovascular Pathology*. Churchill Livingstone, 3 edition, 2001.³
25. D. D. Streeter, H. M. Spotnitz, D. P. Patel, J. Ross, and E. H. Sonnenblick. Fiber Orientation in the Canine Left Ventricle during Diastole and Systole. *Circ. Res.*, 24(3):339–347, 1969.¹
26. H. Sundar, Dinggang Shen, G. Biros, H. Litt, and C. Davatzikos. Estimating Myocardial Fiber Orientations by Template Warping. In *ISBI*, pages 73–76, 2006.¹
27. W.-Y. Y. Tseng, V. J. Wedeen, T. G. Reese, R. N. Smith, and E. F. Halpern. Diffusion tensor MRI of myocardial fibers and sheets: correspondence with visible cut-face texture. *J. of Mag. Res. Im.*, 17(1):31–42, 2003.³
28. A. van Leeuwenhoek. Correspondence with the members of the royal society in london. *Letter no 82*, April 1694.¹
29. T. Vercauteren, X. Pennec, A. Perchant, and N. Ayache. Symmetric Log-Domain Diffeomorphic Registration: A Demons-Based Approach. In *MICCAI*, pages 754–761, 2008.³